2.1 THz quantum-cascade laser operating up to 144 K based on a scattering-assisted injection design

Sudeep Khanal,[1,*] **John L. Reno,**[2] **and Sushil Kumar**[1]

[1]*Department of Electrical Engineering and Computer Science, Lehigh University, Bethlehem, PA 18015, USA*

[2]*Sandia National Laboratories, Center of Integrated Nanotechnologies, MS 1303, Albuquerque, NM 87185-1303, USA*

[*]*suk311@lehigh.edu*

Abstract: A 2.1 THz quantum cascade laser (QCL) based on a scattering-assisted injection and resonant-phonon depopulation design scheme is demonstrated. The QCL is based on a four-well period implemented in the GaAs/$Al_{0.15}Ga_{0.85}As$ material system. The QCL operates up to a heat-sink temperature of 144 K in pulsed-mode, which is considerably higher than that achieved for previously reported THz QCLs operating around the frequency of 2 THz. At 46 K, the threshold current-density was measured as $\sim$ 745 A/cm^2 with a peak-power output of $\sim$ 10 mW. Electrically stable operation in a positive differential-resistance regime is achieved by a careful choice of design parameters. The results validate the robustness of scattering-assisted injection schemes for development of low-frequency ($\nu < 2.5$ THz) QCLs.

OCIS codes: (040.2235) Far infrared or terahertz; (140.5965) Semiconductor lasers, quantum cascade.

References and links

1. R. Köhler, A. Tredicucci, F. Beltram, H. E. Beere, E. H. Linfield, A. G. Davies, D. A. Ritchie, R. C. Iotti, and F. Rossi, "Terahertz semiconductor-heterostructure laser," Nature **417**, 156–159 (2002).
2. B. S. Williams, "Terahertz quantum-cascade lasers," Nat. Photonics **1**, 517–525 (2007).
3. C. Walther, M. Fischer, G. Scalari, R. Terazzi, N. Hoyler, and J. Faist, "Quantum cascade lasers operating from 1.2 to 1.6 THz," Appl. Phys. Lett. **91**, 131122 (2007).
4. C. W. I. Chan, Q. Hu, and J. L. Reno, "Ground state terahertz quantum cascade lasers," Appl. Phys. Lett. **101**, 151108 (2012).
5. S. Fathololoumi, E. Dupont, C. W. I. Chan, Z. R. Wasilewski, S. R. Laframboise, D. Ban, A. Mátyás, C. Jirauschek, Q. Hu, and H. C. Liu, "Terahertz quantum cascade lasers operating up to $\sim$ 200 K with optimized oscillator strength and improved injection tunneling," Opt. Express **20**, 3866 (2012).
6. L. Li, L. Chen, J. Zhu, J. Freeman, P. Dean, A. Valavanis, A. G. Davies, and E. H. Linfield, "Terahertz quantum cascade lasers with $>$ 1 W output powers," Electron. Lett. **50**, 309 (2014).
7. C. Worral, J. Alton, M. Houghton, S. Barbieri, H. E. Beere, D. Ritchie, and C. Sirtori, "Continuous wave operation of a superlattice quantum cascade laser emitting at 2 THz," Opt. Express **14**, 171 (2006).
8. S. Kumar, B. S. Williams, Q. Hu, and J. L. Reno, "1.9 THz quantum-cascade lasers with one-well injector," Appl. Phys. Lett. **88**, 121123 (2006).
9. C. Walther, G. Scalari, J. Faist, H. Beere, and D. Ritchie, "Low frequency terahertz quantum cascade laser operating from 1.6 to 1.8 THz," Appl. Phys. Lett. **89**, 231121 (2006).
10. S. Kumar, C. W. I. Chan, Q. Hu, and J. L. Reno, "A 1.8 THz quantum-cascade laser operating significantly above the temperature of $\hbar\omega/k_B$," Nat. Phys. **7**, 166 (2011).

#238241 Received 16 Apr 2015; revised 17 Jun 2015; accepted 17 Jun 2015; published 22 Jul 2015

11. E. Dupont, S. Fathololoumi, Z. R. Wasilewski, G. Aers, S. R. Laframboise, M. Lindskog, S. G. Razavipour, A. Wacker, D. Ban, and H. C. Liu, "A phonon scattering assisted injection and extraction based terahertz quantum cascade laser," J. Appl. Phys. **111**, 073111 (2012).
12. K. Fujita, M. Yamanishi, S. Furuta, K. Tanaka, T. Edamura, T. Kubis, and G. Klimeck, "Indirectly pumped 3.7 THz InGaAs/InAlAs quantum-cascade lasers grown by metal-organic vapor-phase epitaxy," Opt. Express **20**, 20647 (2012).
13. S. G. Razavipour, E. Dupont, S. Fathololoumi, C. W. I. Chan, M. Lindskog, Z. R. Wasilewski, G. Aers, S. R. Laframboise, A. Wacker, Q. Hu, D. Ban, and H. C. Liu, "An indirectly pumped terahertz quantum cascade laser with low injection coupling strength operating above 150 K," J. Appl. Phys. **113**, 203107 (2013).
14. S. G. Razavipour, E. Dupont, C. W. I. Chan, C. Xu, Z. R. Wasilewski, S. R. Laframboise, Q. Hu, and D. Ban, "A high carrier injection terahertz quantum cascade laser based on indirectly pumped scheme," Appl. Phys. Lett. **104**, 041111 (2014).
15. S. Kumar and Q. Hu, "Coherence of resonant-tunneling transport in terahertz quantum-cascade lasers," Phys. Rev. B **80**, 245316 (2009).
16. H. Yasuda, T. Kubis, P. Vogl, N. Sekine, I. Hosako, and K. Hirakawa, "Nonequilibrium green's function calculation for four-level scheme terahertz quantum cascade lasers," Appl. Phys. Lett. **94**, 151109 (2009).
17. S. Kumar, "Recent progress in terahertz quantum cascade lasers," IEEE IEEE J. Sel. Top. Quantum Electron. **17**, 38 (2011).
18. S. Khanal, L. Zhao, J. L. Reno, and S. Kumar, "Temperature performance of terahertz quantum-cascade lasers with resonant phonon active-regions," J. Opt **16**, 094001 (2014).
19. B. S. Williams, H. Callebaut, S. Kumar, Q. Hu, and J. L. Reno, "3.4-THz quantum cascade laser based on longitudinal-optical-phonon scattering for depopulation," Appl. Phys. Lett. **82**, 1015–1017 (2003).
20. R. S. Dhar, S. G. Razavipour, E. Dupont, C. Xu, S. Laframboise, Z. Wasilewski, Q. Hu, and D. Ban, "Direct nanoscale imaging of evolving electric field domains in quantum structures," Sci. Rep. **4**, 7183 (2014).
21. S. Kumar, "Development of terahertz quantum-cascade lasers," PhD dissertation, Massachusetts Institute of Technology, Department of Electrical Engineering and Computer Science (2007).

1. Introduction

The terahertz (THz)/far-infrared region of the spectrum ($\nu \sim 1-10$ THz, $\lambda \sim 30-300$ μm, photon energy $h\nu \sim 4-40$ meV) is ideal in many ways for chemical and biological sensing, imaging, and spectroscopy. Many molecular species have very strong characteristic THz rotational and ro-vibrational transitions (both inter and intra-molecular), and hence could be "fingerprinted" with THz spectroscopy. The low-frequency THz spectral region, specifically $\nu \sim 1-2$ THz, will find important applications in the general areas of defense and security. This spectral region provides some low-loss atmospheric transmission windows in which THz sensing and detection is possible for short-range standoff distances (up to 100 m). Also materials such as clothing, ceramics, and plastics are semi-transparent at low-THz frequencies while the wavelength is shorter than microwaves to allow good spatial resolution with small aperture devices, for potential development of hand-held sensing/imaging systems. Owing to the specific rotational/vibrational spectral features of molecules, THz radiation could potentially be used for short-range radar-sensing applications for spectroscopic identification of buried, hidden, or packaged explosives, or other chemical and biological threat agents.

THz quantum-cascade lasers (QCLs) that were invented in 2001 [1,2] are the most powerful solid-state sources of coherent THz radiation. Today, THz QCLs have been designed to emit in a broad frequency range of 1.2 THz [3] to 5.2 THz [4]. However, they require cryogenic cooling which limits their use for practical applications. Portable electrically-operated cryocoolers are now commercially available that could provide considerable cooling power at temperatures in the range of $70-100$ K, hence if good QCL performance (power output, spectral and modal characteristics) could be achieved at such temperatures, development of commercial QCL-based THz instruments will be a possibility. The maximum operating temperature of the QCLs should be much greater than 100 K to achieve such a capability.

The maximum operating temperature of THz QCLs is not consistently high across the entire frequency range and depends significantly on the emission frequency as well as on the design scheme. The best performing THz QCLs operate at frequencies $\nu \gtrsim 3$ THz based on *resonant-*

#238241 Received 16 Apr 2015; revised 17 Jun 2015; accepted 17 Jun 2015; published 22 Jul 2015

tunneling (RT) injection and resonant-phonon depopulation [2]. Operation up to a temperature of ∼200 K was realized for emission frequency of ∼3.2 THz [5] in the GaAs/$Al_{0.15}Ga_{0.85}As$ material system. Peak optical power output in excess of 1 W at 10 K was reported recently for a 3.4 THz QCL [6]. For low-frequency QCLs, however, the maximum operating temperatures are much lower. For QCLs designed for emission close to (or below) 2 THz, the best reported values are in the range of $75-110$ K [7–9] based on designs with RT injection. It is well known that QCLs emitting at or below 2 THz are difficult to design and may require multiple growth iterations of an exact same design that may have worked in the past. This is exemplified by the fact that these are almost a decade old results and that only few such QCLs have been experimentally realized. Recently, there was a demonstration of a low-frequency ($\nu \sim 1.8$ THz) QCL that operated up to a significantly higher temperature (163 K) based on a *scattering-assisted* (SA) design technique [10]. The first demonstration of a THz QCL with SA technique in Ref. [10] was not ideal, because the device showed undesired dual-color lasing, and more-importantly, the low-frequency emission occurred partially in the electrically unstable bias region with a negative differential-resistance. Since then, several other THz QCLs based on SA injection have been demonstrated as referenced chronologically in Table 1. However, all such latter developments of THz QCLs with SA injection have focused on designs operating at higher-frequencies where QCLs based on RT injection also perform equally well (or better). The objective of this work is to demonstrate that SA injection is a better choice for design of low-frequency THz QCLs. A 2.1 THz QCL operating up to a temperature of 144 K is realized, which is significantly better than the previous-best of 77 K for a QCL operating at similar frequency [7], and is the best reported value for any THz QCL operating in the frequency range of $1.9-2.3$ THz.

Table 1. THz QCLs with scattering-assisted (SA) injection listed in chronological order of development. The key design and performance parameters are indicated.

Design	Material system	Frequency	T_{max}	#wells/ #subbands	J_{th}@ 10 K (A/cm^2)
Kumar *et al.* [10]	GaAs/$Al_{0.15}Ga_{0.85}As$	1.8 THz	163 K	4/5	865
Dupont *et al.* [11]	GaAs/$Al_{0.25}Ga_{0.75}As$	3.2 THz	138 K	4/4	1170
Fujita *et al.* [12]	$In_{0.53}Ga_{0.47}As/In_{0.52}Al_{0.48}As$	3.7 THz	100 K	5/6	420
Razavipour *et al.* [13]	GaAs/$Al_{0.25}Ga_{0.75}As$	2.4 THz	153 K	4/4	800
Razavipour *et al.* [14]	GaAs/$Al_{0.25}Ga_{0.75}As$	2.67 THz	151 K	5/4	1440
This work	GaAs/$Al_{0.15}Ga_{0.85}As$	2.1 THz	144 K	4/5	745 (46 K)

2. THz QCLs with scattering-assisted injection

Most design schemes for THz QCLs involve resonant-tunneling (RT) injection into the upper laser subband. However, there are two major drawbacks of the RT injection scheme. First, at the bias corresponding to maximum gain, the electrons from injector subband tunnel to the upper laser subband which implies that at bias corresponding to resonant-alignment, a maximum of 50% of available electrons could be injected into the upper lasing subband (in ideal case).

#238241 Received 16 Apr 2015; revised 17 Jun 2015; accepted 17 Jun 2015; published 22 Jul 2015

In reality, the tunnel coupling between injector and upper laser subbands has to be kept weak for THz QCLs [15], and hence, the ratio of population inversion to total electron-population is much less than 50% [11,16]. Second, for low-frequency designs, the energy separation between upper and lower lasing subbands is small and is close in magnitude to the energy broadening of subbands, which limits the selective injection from injector subband to the upper-lasing subband [10]. Such limitations of RT scheme could be overcome by scattering-assisted (SA) injection (also referred as indirect pumping [16]) where electron-injection into the upper radiative subband is facilitated by the fast electron-LO-phonon scattering. As compared to the RT scheme, the potential barrier that limits flow of current through the QCL structure the most, could be made much thinner in the SA scheme. Not only does this increase the output power of the QCL, but it also increases the dynamic range of current (difference between *maximum current* and *threshold current*), which leads to better temperature performance for the QCL [17]. This is evident when comparing the $1.8-1.9$ THz QCLs in Refs. [8, 9] with RT injection to the 1.8 THz QCL in Ref. [10] with SA injection. The QCLs with RT scheme had a maximum operating temperature in the range of $95-110$ K, whereas the QCL with SA scheme had a greater dynamic range for lasing and operated up to a temperature of 163 K.

The 1.8 THz QCL with SA scheme in Ref. [10] suffered from two problems: dual-color lasing ($\sim$ 1.8 THz and $\sim$ 4 THz), and lasing at $\sim$ 1.8 THz occurring predominantly in the negative differential-resistance (NDR) region of the QCL's *I-V* characteristics. The dual-color lasing occurred due to the fact that the intersubband transition responsible for SA injection also results in intersubband gain due to a population inversion that could easily develop between the injector subbands and the desired upper radiative subband. Since shallow barriers with 15 % Al content were used, the intersubband energy separation between injector and upper radiative subband was kept much below the LO-phonon energy, which allows lasing to occur for that transition should intersubband gain be established. The dual-color lasing also leads to early occurrence of NDR prior to the desired "design" bias condition since stimulated transition due to undesired lasing process leads to higher than desired current flow prior to the designed bias. THz QCLs with SA scheme since the original demonstration in Ref. [10] have focused on designs with taller barriers (i. e. greater than 15 % content in AlGaAs barriers) as evident from Table 1. Additionally, all those subsequent designs have focused on high-frequency operation ($\nu \gtrsim 2.4$ THz) where RT schemes typically provide better temperature performance.

The objective of this work is to demonstrate that the original design scheme of Ref. [10] for low-frequency THz QCLs with SA injection could indeed be implemented with 15 % Al content barriers while eliminating the undesired dual-color lasing effect, and also to achieve lasing operation in the stable bias region of the QCL's *I-V* characteristics. We achieve those objectives by making some important changes to the four-well design of Ref. [10], while keeping the overall injection and depopulation schemes as well as number of wells and subbands the same as before. This includes making the intersubband energy separation for injection closer to the LO-phonon energy, and making it more diagonal, as well as making the desired radiative transition more diagonal. Lasing at 2.1 THz is realized up to a maximum operating temperature of 144 K with a comparatively lower threshold current-density than that of previously demonstrated THz QCLs with SA injection in the GaAs/AlGaAs material system.

3. Design and fabrication

The SA injection scheme requires a large operating electric-field across the QCL superlattice in contrast with the RT scheme for design of THz QCLs. This makes it difficult to implement the SA scheme with $Al_{0.15}Ga_{0.85}As$ barriers (barrier-height $\sim$ 135 meV) when the QCL is designed for emission at higher frequencies. Consequently, all but the initial demonstration for THz QCLs with SA scheme utilized superlattices with taller barriers as can be noted from Ta-

#238241 Received 16 Apr 2015; revised 17 Jun 2015; accepted 17 Jun 2015; published 22 Jul 2015

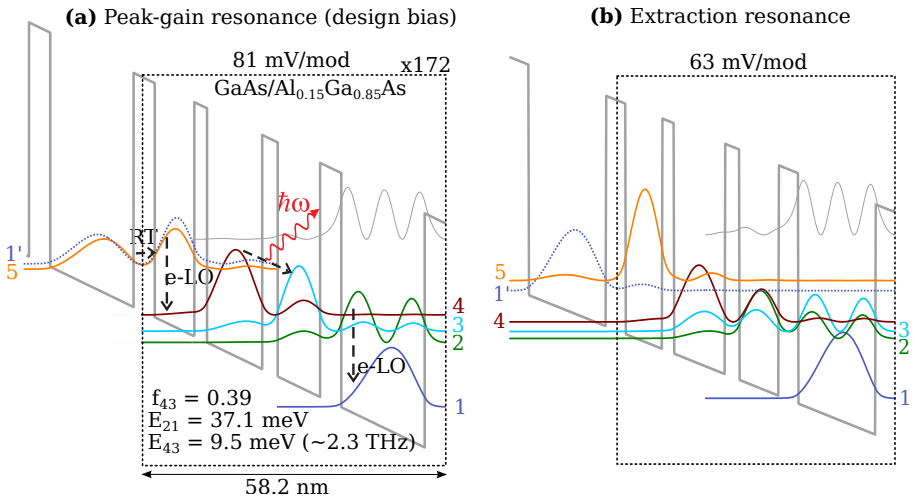

Fig. 1. Conduction-band diagrams for design SARP172 at two different biases where the repeat-structure with four-wells is highlighted. Starting from leftmost barrier of the period, the layer thicknesses in nm (with barriers indicated in bold-face font) are **4.24**/8.48/**3.11**/11.02/**2.54**/7.91/**4.24**/16.67 and the widest well is n-doped with Si at 1.9×10^{16} cm^{-3}. The average doping in the active region is 5.44×10^{15} cm^{-3} (3.17×10^{10} cm^{-2} per period). (a) Band diagram at design-bias corresponding to peak-gain condition, at 81 mV/module (1.39×10^6 V/m). The radiative transition is from subband $4 \rightarrow 3$. (b) Band diagram at a lower bias of 63 mV/module that corresponds to the extraction resonance for resonant-phonon depopulation scheme where lower radiative subband 3 aligns with subband 2 in the adjacent well (energy splitting ~ 4.1 meV).

ble 1. However, designs with tall-barriers have to employ thinner barriers to maintain optimum carrier transport, which increases interface-roughness scattering that may worsen the QCL's performance [18]. Hence, for this implementation, $Al_{0.15}Ga_{0.85}As$ barriers were chosen for the superlattice as in Ref. [10].

Figure 1 shows the conduction-band diagram of the design named SARP172 (wafer VA0344) at two relevant bias conditions in which intersubband gain is realized. The structure was grown in the GaAs/$Al_{0.15}Ga_{0.85}As$ material system with 172 cascaded periods yielding an overall thickness of ~ 10 μm for the active-region. Structure SARP172 is a modification of the first reported THz QCL with SA scheme in Ref. [10]. It utilizes similar design scheme of four-wells per period, in which predominantly five subbands take part in carrier transport. The carriers are injected from an anticrossed doublet of subbands ($1' - 5$, energy splitting at resonance $E_{1'5} \sim 3.1$ meV) into the upper radiative subband 4 by electron-LO-phonon scattering ($E_{54} \sim 28.5$ meV). The radiative transition is from subband 4 to 3 ($E_{43} \sim 9.5$ meV at the designed bias), and the lower radiative subband 3 is depopulated by the resonant-phonon depopulation process [19].

Several changes are made to the key design parameters of the original design in Ref. [10] to achieve lasing in a positive-differential resistance regime and also to suppress the undesired high-frequency lasing operation from injector subband 5 to 4. First, the energy separation between the injector subband 5 and upper laser subband 4 was increased (28.5 meV instead of 20 meV), which makes it much closer to the GaAs LO-phonon energy of 36 meV and eliminates the possibility of a radiative transition at that energy. Second, the radiative oscillator strength f_{43} was reduced (~ 0.39 instead of 0.60) to make the design more diagonal, which improves selectivity of injection into the upper laser subband. Finally, the $3-2$ alignment was purposefully

#238241 Received 16 Apr 2015; revised 17 Jun 2015; accepted 17 Jun 2015; published 22 Jul 2015

detuned from its resonant-alignment at the designated design-bias, which is determined by the bias corresponding to $1' - 5$ alignment since it leads to maximum current transport. Such an alignment allows the $3 - 2$ resonance to occur at a lower-bias (63 mV/module as opposed to the design-bias of 81 mV/module, as shown in Fig. 1(b), and hence, a population inversion could be established at a much lower voltage. This ensures that the lasing threshold is achieved at a lower current-density and also serves to increase the dynamic range for lasing in the *I-V* characteristics. Metal-metal ridge-waveguide lasers were processed similarly as mentioned in Ref. [8] but with Ta/Cu/Au as top metal and the ridges were wet-etched using 1:8:80 H_2SO_4:H_2O_2:H_2O solution. For thermo-compression bonding, Ta/Cu layers were used on both the substrate wafer as well as the MBE grown QCL wafer. After cleaving, the QCL-chip was indium soldered on a copper mount and was mounted on the cold plate of a cryocooler for characterization.

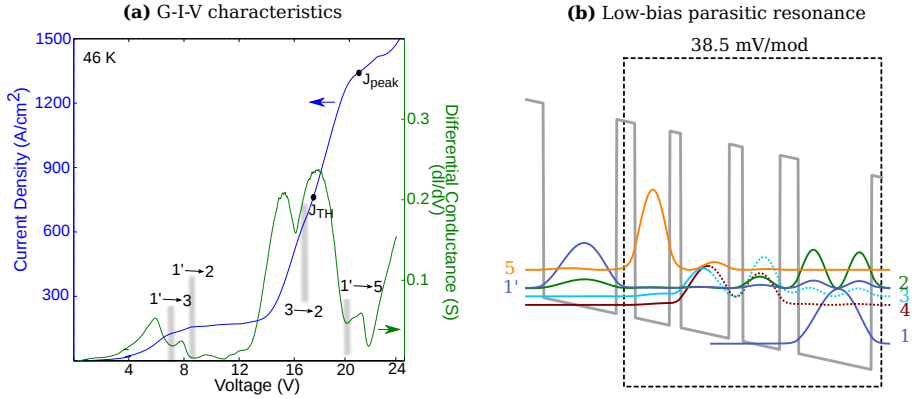

Fig. 2. (a) Experimental results from a representative Fabry-Pérot cavity QCL. Pulsed *I-V* characteristic at 46 K from a 0.64 mm $\times$ 150 μm ridge laser is shown with blue line. The locations of threshold ($J_{\text{th}} \sim 745$ A/cm^2) and peak-power ($J_{\text{peak}} \sim 1350$ A/cm^2) current-density are indicated. Digitized *G-V* characteristic of the same device is shown with green line. The occurrence of valleys on the *G-V* curve correspond approximately to bias that leads to local maxima in current-transport due to resonant-tunneling alignments of different subbands as indicated. (b) Conduction-band diagram of the QCL structure when biased at 38.5 mV/module, which corresponds to a low-bias parasitic current channel due to the 1'→2 subband alignment [8].

4. Results

Figure 2(a) shows pulsed *I-V* and *G-V* (differential conductance versus voltage) characteristics of a representative ridge-cavity QCL fabricated from the grown wafer, measured at a heat-sink temperature of 46 K. The threshold current-density at this temperature was $J_{\text{th}} \sim 745$ A/cm^2 and the peak-power output for the QCL occurs at $J_{\text{peak}} \sim 1350$ A/cm^2, which are both marked as dots respectively on the *I-V* curve. The differential-conductance G (slope of the *I-V* curve) highlights some of the key transport characteristics of this QCL. Each conductance peak could be associated with a specific resonant-tunneling alignment that facilitates current flow across the QCL superlattice. The resonance condition leads to a local maxima in the *I-V* curve, which corresponds to a local minima in the *G-V* curve. The lasing threshold is achieved soon after the $3 - 2$ extraction resonance (~ 17 V) beyond which majority of the current flow occurs due to $1' \rightarrow 5$ tunneling and $5 \rightarrow (4, 3)$ non-radiative scattering assisted by LO-phonon emission. Unlike THz QCLs based on RT injection [15], no discontinuity in the *G-V* curve was observed at threshold for this QCL [11]. This is likely due to the fact that current transport across the QCL

#238241 Received 16 Apr 2015; revised 17 Jun 2015; accepted 17 Jun 2015; published 22 Jul 2015

superlattice is dominated by the overall lifetime of subbands $1'$ and 5, and the reduction in the lifetime of upper radiative subband 4 due to stimulated radiative transitions does not alter net current flow significantly. The peak-power output occurs close to the $1'-5$ resonance condition ($\sim$ 20 V), beyond which the *I-V* enters an NDR regime and a homogeneous bias condition could no longer be maintained across the QCL's superlattice. The QCL does not show an NDR region prior to the peak-power bias in contrast to the device in Ref. [10] since the undesired $5 \rightarrow 4$ lasing is eliminated, which was one of the primary goals of this modified design. It may be noted that the threshold and peak-power operating voltages for the QCL are much higher than the expected values. From Fig. 1, the extraction resonance should occur at $\sim$ 10.9 V (63 mV/module) and the design-bias alignment should occur at $\sim$ 13.9 V (81 mV/module). However, the measured *G-V* curve indicates that the corresponding resonances occur at almost $\sim$ 6 V in excess of the expected values. The origin of the extra voltage drop in the active region is likely due to high-field domain formation in the active region that is discussed next.

The *I-V* curve of this QCL reveals an occurrence of a current-plateau starting at $\sim$ 8 V. Assuming $\sim 1-2$ V is dropped at the QCL's Schottky contacts, the current plateau corresponds to a low-bias parasitic current channel alignment of subbands $1'-2$, which should occur at 38.5 mV/module corresponding to $\sim$ 6.6 V across the active region. For resonant-phonon THz QCLs based on RT injection, this parasitic current channel could often lead to an early occurrence of an NDR in the *I-V* curve and is typically minimized by keeping the tunneling barriers thick [8]. For designs based on SA injection, current-density at this alignment is automatically small owing to the fact that such a alignment occurs at a significantly lower bias compared to the operating (design) bias, when subbands are located at low energies in the wells and have weak inter-well tunnel couplings. Nevertheless, beyond the $1'-2$ alignment, theoretically the current should drop with increasing voltage in the *I-V* curve since the next alignment for current flow is that of the desired $1'-5$ alignment that occurs at a much higher voltage. Such a local drop of current could lead to occurrence of high-field domains in the QCL's superlattice, which was also recently confirmed experimentally for THz QCLs with SA injection scheme using scanning voltage microscopy [20]. It was observed that not all of the QCL modules maintain homogeneous electric-field in this bias region. Likewise, it is expected that the shown device enters such a regime at that bias ($\sim$ 8 V), that leads to the occurrence of an extended current plateau in the *I-V* curve. As the bias is increased further, QCL modules gradually come out of high-field domain formation and majority of the superlattice is in uniform field regime again prior to the occurrence of threshold. However, the fact that few QCL modules may still be biased at high-fields [20] in the superlattice could possibly explain the considerable increase in the threshold and peak-power operating voltages of the QCL compared to the expected values based on the band diagrams of Fig. 1.

Figure 3 shows the pulsed *L-I* characteristics as well as spectra from a representative edge-emitting Fabry-Pérot cavity QCL as a function of varying heat-sink temperatures (T). The QCL lased up to a maximum temperature of 144 K. At low-temperatures $\sim$ 10 mW of peak output power was detected with a calibrated power meter. Figure 3(b) shows representative spectra of the QCL close to threshold for different temperatures. At 46 K, the QCL lased at $\sim$ 2.07 THz when biased close to threshold at 750 A/cm^2. The emission frequency changes to $\sim$ 2.14 THz close to the the peak current-density at 1350 A/cm^2. Owing to the small Stark-shift in the gain spectrum with increasing threshold current-densities at higher temperatures, QCL's emission stays close to the high frequency value. Close to the highest operating temperature at 141 K, the emission frequency shifts to $\sim$ 2.2 THz. Overall, the lasing frequency spans a relatively small range of $2.1-2.2$ THz, which is slightly lower than the designed radiative separation of 2.3 THz for the maximum-gain bias condition. The effect of Stark-shift with increasing bias is less pronounced for this QCL in its emission spectrum as compared to typical THz QCLs

#238241 Received 16 Apr 2015; revised 17 Jun 2015; accepted 17 Jun 2015; published 22 Jul 2015

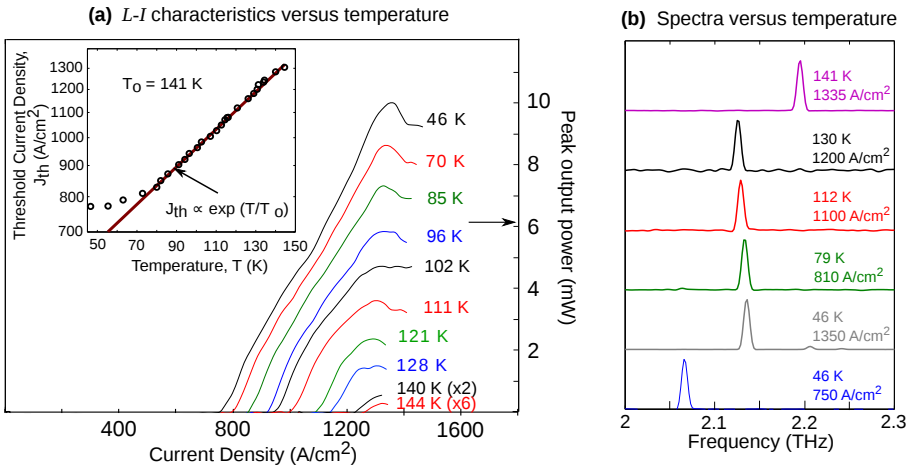

Fig. 3. (a) Pulsed *L-I* characteristics from the representative Fabry-Pérot cavity QCL of dimensions 0.64 mm $\times$ 150 μm plotted as a function of heat-sink temperature T. The measurements were performed with 200 ns current pulses repeated at 100 kHz. The *L-I* data was recorded with a pyroelectric detector. The peak optical power is calibrated using a thermopile power meter placed face-to-face with the cryocooler window without any corrections for collected power. Upper inset shows the threshold current-density ($J_{\rm th}$) versus T plotted on a semi-logarithmic scale. A phenomenological fit to the expression $J_{\rm th} \propto \exp(T/T_0)$ is indicated by a straight line, which results in a value of $T_0 = 141$ K. (b) Representative spectra from the device measured close to threshold at different heat-sink temperatures. For 46 K, spectrum close to the peak current-density is also shown. The spectra were measured using a Bruker 70v Fourier-transform spectrometer under vacuum with the QCL biased with current pulses at 2% duty-cycle. The QCL structure was designed to lase in the frequency range of $\sim 2.0-2.3$ THz (radiative-separation is Stark-shifted from ~ 2 THz to 2.2 THz from low-bias to design-bias). The QCL achieves lasing predominantly at a frequency of 2.1 THz. At 46 , the center frequency of the emission is at 2.07 THz around threshold (~ 750 A/cm^2), which shifts to ~ 2.14 THz at the peak current-density (~ 1350 A/cm^2), which confirms that emission is entirely due to the $4 \rightarrow 3$ radiative transition.

based on RT injection. This suggests that the electric-field across wells localizing the radiative subbands does not change significantly across the range of operation in its *I-V* characteristics.

The energy separation between injector subband 5 and upper radiative subband 4 was increased for design SARP172 as compared to its parent design in Ref. [10]. This should lead to a better injection efficiency owing to the shorter lifetime due to LO-phonon scattering $5 \rightarrow 4$, which is calculated to be 2.3 ps at a lattice temperature of 77 K and an assumed electron temperature of 150 K in subband 5 as compared to a value of 3.0 ps for the design in Ref. [10]. Additionally, the radiative transition $4 \rightarrow 3$ was made more diagonal to improve the injection selectivity, which could be characterized by the lifetime ratio τ_{53}/τ_{54} that is calculated to be 2.3 for SARP172 as opposed to a value of 1.3 for the design in Ref. [10]. However, despite these design improvements, the maximum operating temperature for SARP172 is slightly worse than that of its parent design. A likely reason for this is due to the fact that the injector subband 5 is energetically located close to the energy continuum over the potential barriers, that could lead to carrier leakage at high temperatures. Such a leakage mechanism is difficult to quantify and no accurate models exist to model such an effect for THz QCLs. The carrier leakage over barriers could be reduced by utilizing taller barriers as has been done for all other reports for THz

#238241 Received 16 Apr 2015; revised 17 Jun 2015; accepted 17 Jun 2015; published 22 Jul 2015

QCLs based on SA injection. However, taller barriers lead to greater role of interface-roughness scattering, and have clearly not led to significant improvement in temperature performance as evident from the summary in Table 1.

The variation of J_{th} vs. T in the *L-I* characteristics can provide some additional information about the QCL. The variation is typically characterized by the parameter T_0 according to the fit to exponential relation $J_{\text{th}} \propto \exp(T/T_0)$. A T_0 value of ~ 140 K for this QCL is relatively similar to that of other best-performing QCLs with the RT scheme that operate around 3 THz [21]. It must be noted that the J_{th} increases more rapidly with temperature (leading to a smaller T_0) in QCLs operating at higher frequencies. In such cases, the subband(s) taking part in electron-transport are energetically located higher in the quantum-wells, from where electron leakage into continuum over the barriers causes a rapid degradation in intersubband gain [18]. A large T_0 for this QCL suggests the shallow barrier height in the GaAs/$Al_{0.15}Ga_{0.85}$As material-system is not yet a deterrent to temperature performance, and that it may be possible to implement SA scheme in the GaAs/$Al_{0.15}Ga_{0.85}$As material-system for higher-frequency THz QCLs as well. Finally, it must be noted that THz QCLs based on SA injection typically have larger operating current-densities, which is true for SARP172 as well when compared to QCLs based on RT injection and operating close to 2 THz [8]. This is primarily because a large parallel current path exists in the QCL structure due to $5 \rightarrow 3 \rightarrow 2$ non-radiative scattering and tunneling process, which by-passes the $4 \rightarrow 3$ radiative transition. Additionally, the operating voltage for this design is significantly greater than that for bound-to-continuum designs [7, 9]. Both of these effects lower the quantum-efficiency of THz QCLs based on SA injection significantly. For example, the single-facet peak wall-plug efficiency of SARP172 was calculated as 0.04%, while for the 2 THz QCL designed with bound-to-continuum scheme, it is calculated as 1.7% [7]. In general, the wall-plug efficiency of the QCL discussed in this article is lower than that of the best performing THz QCLs based on RT injection schemes. However, for THz QCLs, wall-plug efficiency is relatively a much less significant parameter of practical importance when compared to their maximum operating temperatures, which is the primary motivation for developing THz QCLs based on the SA injection method.

5. Conclusions

Here we presented a 2.1 THz QCL based on a scattering-assisted injection scheme in the GaAs/$Al_{0.15}Ga_{0.85}$As material system. We have found little evidence of increased carrier leakage for the SA scheme implemented with shallow barriers (i. e. low-Al content in the barriers). Hence, GaAs/$Al_{0.15}Ga_{0.85}$As THz QCLs with SA injection design scheme provide optimum temperature performance especially for low-frequency emission. With proper design strategy, we were able to achieve lasing in an electrically stable bias regime with positive differential-resistance. At 46 K, the threshold current density for a representative ridge-cavity QCL was measured as ~ 745 A/cm^2 and the peak current-density was ~ 1350 A/cm^2. The relatively large dynamic range results in a maximum operating temperature of 144 K for the QCL, which is the highest reported value for a QCL operating in this frequency range.

Acknowledgments

This material is based upon work supported by the United States National Science Foundation under Grant Nos. ECCS 1128562 and ECCS 1351142. The work is also performed, in part, at the Center for Integrated Nanotechnologies, a U.S. Department of Energy (DOE), Office of Basic Energy Sciences user facility. Sandia National Laboratories is a multiprogram laboratory managed and operated by Sandia Corporation, a wholly owned subsidiary of Lockheed Martin Corporation, for the U.S. DOE's National Nuclear Security Administration under contract DE-AC04-94AL85000.

#238241 Received 16 Apr 2015; revised 17 Jun 2015; accepted 17 Jun 2015; published 22 Jul 2015